Astron. Astrophys. 346, 947–954 (1999)

ASTRONOMY AND ASTROPHYSICS

Expansion and turbulence in the Hourglass region of the Lagoon Nebula (M 8)

New [OIII]5007Å line observations

A. Chakraborty[⋆] **and B.G. Anandarao**

Physical Research Laboratory, Ahmedabad 380009, India

Received 30 December 1997 / Accepted 1 April 1999

Abstract. We present new, seeing-limited Imaging Fabry-Perot spectroscopic observations in the [OIII]5007Å line in the Hourglass region of the Lagoon nebula. As many as 900 line profiles were obtained in a region of $1' \times 1'$ surrounding the Hourglass, each one representing a spatial element of $2'' \times 2''$. We find expansion of the HII region and high velocities upto $-35\,\mathrm{km\,s^{-1}}$, which indicate Champagne flow. Our observations constrain the orientation of cavities in the Hourglass relative to the line of sight. We identify three kinematically distinct regions in and around the Hourglass. Further, we studied turbulence in the Hourglass region by computing the structure function using a larger set of data points at a resolution of $1''$. We find a power index of 0.46 for the structure function which is in variance with Kolmogoroff's theory.

Key words: ISM: individual objects: M 8 – line: profiles – turbulence – ISM: kinematics and dynamics

1. Introduction

The Lagoon nebula (M 8), one of the closest and the brightest galactic HII regions, is located at a distance of 1.5 kpc in the Sagittarius/Carina spiral arm of the Galaxy (Georgelin & Georgelin 1976). It consists of a HII region (NGC 6523) and a young (2×10^6 yr; Lang 1991) open cluster, NGC6530. The cluster is at the centre of the Sgr OB1 association and is extensively studied by van Altena & Jones (1972). The prominent members of the cluster are the O type stars, 9 Sgr and HD165052. A structure, called "the Hourglass" (HG), having the highest surface brightness and an angular extent of $30''$ in the NS and $15''$ in the EW, is situated near the centre of the optical nebulosity of M 8 (Lada et al. 1976). The study of Woodward et al. (1986) showed that the HG is seen in the optical wavelengths as a bipolar structure, due to varying extinction along the line of sight. Further, Woodward et al. (1990) showed evidence for recent star formation activity in the HG region. Herschel 36 (Her 36), an $O7$V type star, located $15''$ west of the waist of the HG, is found to be responsible for ionizing the region (while the extended region of the Lagoon nebula is ionized by the O type stars, 9 Sgr and HD165052) (Woolf 1961; Elliot et al. 1984; White et al. 1997). It is evident that the region of the HG and Her 36 is very young $\sim 10^4$ yr (Woolf, 1961; Chakraborty & Anandarao, 1997).

The kinematic studies made earlier on M 8 using optical emission lines covered the entire extent of the nebula at a rather low spatial resolution (Bohuski 1973; Goudis & Meaburn 1976; Elliot et al. 1984; Hanel 1987). These studies revealed asymmetric or two-component line profiles of relatively large widths, except towards 9 Sgr (O'Dell et al. 1987). Hanel (1987) reached a general conclusion that the kinematics of the nebula cannot be explained by a simple model that assumes spherically symmetric expansion. Recently Chakraborty & Anandarao (1997, hereafter CA) found evidence for asymmetric expansion and Champagne flow from their [NII] line velocity field observations of the HG region. These results lend support to the structural complexities of the region as revealed in the HST image of the HG and Her 36 (Ref. STScI Homepage). We present here new kinematic observations covering the region of the HG and Her 36 in the [OIII]5007Å emission line using an imaging Fabry-Perot spectrometer ($IFPS$) in the continuous scanning mode. Such a data base is currently non-existent and is necessary to get an insight into the dynamics of the high excitation regions in the Her 36 bubble. It also gives us an opportunity to study the turbulence in the region which was not done so far. Further, we can compare the dynamics of high excitation regions with the relatively low excitation regions probed by the [NII] line (CA). Sect. 2 describes the observations and data analysis. Sect. 3 details the results obtained and we discuss these results in Sect. 4. Conclusions are given in Sect. 5.

2. Observations and data analysis

The regions of the HG and Her 36 were observed in the [OIII]5007Å emission line using the Imaging Fabry-Perot Spectrometer ($IFPS$, Seema et al. 1992). The $IFPS$ was attached at the cassegrain focus (f/13 beam) of the 1.2m telescope at

Send offprint requests to: Anandarao (anand@prl.ernet.in)

⋆ *Present Address:* Inter-University Centre for Astronomy and Astrophysics, Ganeshkhind, Pune – 411007, India (abhijit@iucaa.ernet.in)

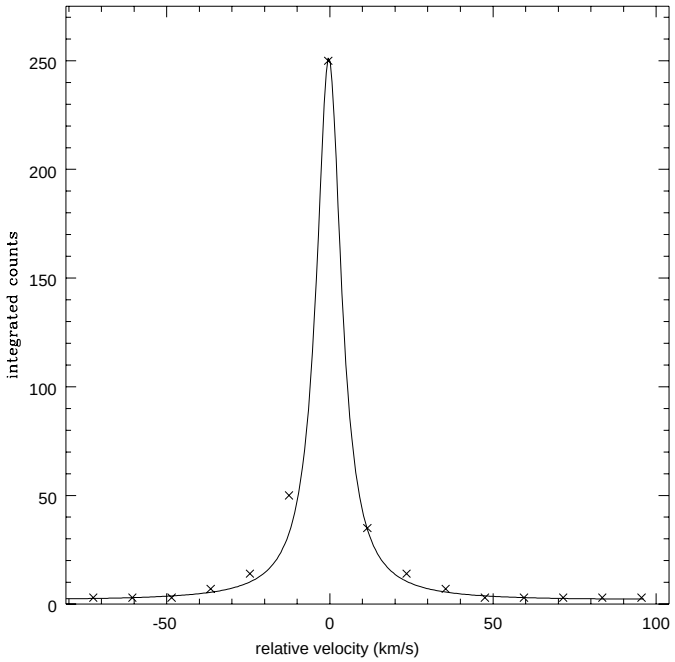

Fig. 1. The instrumental profile at 5015Å

Mt.Abu, India. The observations were made in steady sky conditions with a seeing of 2″. The object was guided by an offset star (9 Sgr), ensuring tracking accuracies of 1″.

A piezo-electrically controlled Fabry-Perot etalon of cavity gap of 416μm (corresponding to a free spectral range (fsr) of 180 km s^{-1} at 5007Å) was used. It was found that the stability of the etalon was better than 1 km s^{-1}. The etalon had an overall effective finesse of 15 and a velocity resolution of 12 km s^{-1}. A data cube was generated in wavelength by scanning the etalon for one fsr with a step increment of 12 km s^{-1}. Thus, the raw data cube consists of 15 interferograms and represents a rather under-sampled spectral data. This under-sampling was forced due to the unpredictability of the sky conditions in India during summer months when the object is accessible. The criterion was to complete observations in a single, clear and steady night with a good seeing. The images were recorded on an Imaging Photon Detector (IPD) manufactured by Photek Ltd., UK. Each of the raw images was digitized by a software (supplied by Photek) to obtain an array of size 512×512, with a pixel size of 35 μm which corresponds to one arcsec on the sky.

Each interferogram was integrated for 10 mt to achieve a S/N ratio of 20 to 30. Dark frames of equal integration time were also recorded before and after the observations. A mean of such dark frames was subtracted from each of the 15 interferograms. These dark-subtracted interferograms were used to build up phase-corrected line profiles for every 2×2 ($2''\times2''$) pixels by the process described by Atherton et al. (1982). A phase-corrected instrumental profile generated from 15 standard interferograms on the HeI line 5015Å is shown in Fig. 1. We processed a total of 900 profiles over a matrix size of 60×60 pixels ($1'\times1'$) covering the region of HG and Her 36. Assuming that an emission line profile is represented by a gaussian, each of the observed profiles was analysed using a multi-gaussian fitting software (Anandarao & Rao 1985) to obtain peak position, amplitude and width. The wavelength calibration was done from interferograms recorded on standard laboratory sources. As a confirmatory test, we have made FPS observations towards 9 Sgr for which the radial velocity is known in the literature (Elliot et al. 1984; O'Dell et al. 1987) along with Her 36 and found that their radial velocities are the same within errors of observation. From our analysis, we obtain a [OIII] heliocentric velocity of -5.0 ± 2 km s^{-1} for Her 36. The peak positions in terms of heliocentric velocity at different points were then determined using the calibration on Her 36. The error in finding the peak positions (centroiding) was $\pm$ 2 km s^{-1}. Since the spectral line was under-sampled in steps of instrumental width (12 km s^{-1}), it would probably be inappropriate to comment on blended or asymmetric lines within 12 km s^{-1}. However, split profiles with components separated by 20 km s^{-1} or more were considered for discussion.

3. Results and discussion

Our observations revealed a variety of line profile shapes which included symmetric and single component profiles, asymmetric profiles, and clearly split multicomponent profiles (the full sample is given in Chakraborty 1997). The number of the clear double (75) or triple (9) peaked profiles constitutes only a small fraction of the total number (900) observed. Fig. 2 shows a sample of twelve line profiles, the spatial positions of which are marked on the top of the plots as offsets in RA and Dec in arcsec measured from Her 36. The velocity scale is shown in heliocentric values. One can notice in the figure the unambiguous split in some of the line profiles with peak-to-peak separations of more than 20 km s^{-1}. For comparison, a single component profile is shown at the top left corner of the figure. A few samples of more complex triple component profiles are also shown; however, such profiles are very few and found in a small clumpy region about 5 arcsec south-east of Her 36.

Fig. 3 shows a velocity map of the region constructed from the peak positions of the primary components of the line profiles. The heliocentric velocity contours are labeled in km s^{-1}. The $X-$ and $Y-$axes are the offsets in right ascension and declination respectively (given in arcsec from Her 36; positive sign represents West in RA and North in Dec). An HST [OIII] image of the HG region (obtained from the STScI homepage) is also shown superposed on the velocity map in the figure. The velocity map identifies three kinematically distinct regions: (a) the Northern HG (NHG), (b) the Southern HG (SHG) and the region south of Her 36, and (c) the region west of Her 36. While the NHG region shows positive radial velocities upto 15 km s^{-1}, the SHG and the region south of Her 36 show distinct split profiles and negative velocities upto -35 km s^{-1}. Regions west of Her 36 show velocities upto -17 km s^{-1}. The velocity gradient from NHG to SHG was found to be smooth and gradual.

In the following subsections, we discuss three important aspects of our results, $viz.$ the expansion of the HII region, the high velocity flows and the turbulence characterization.

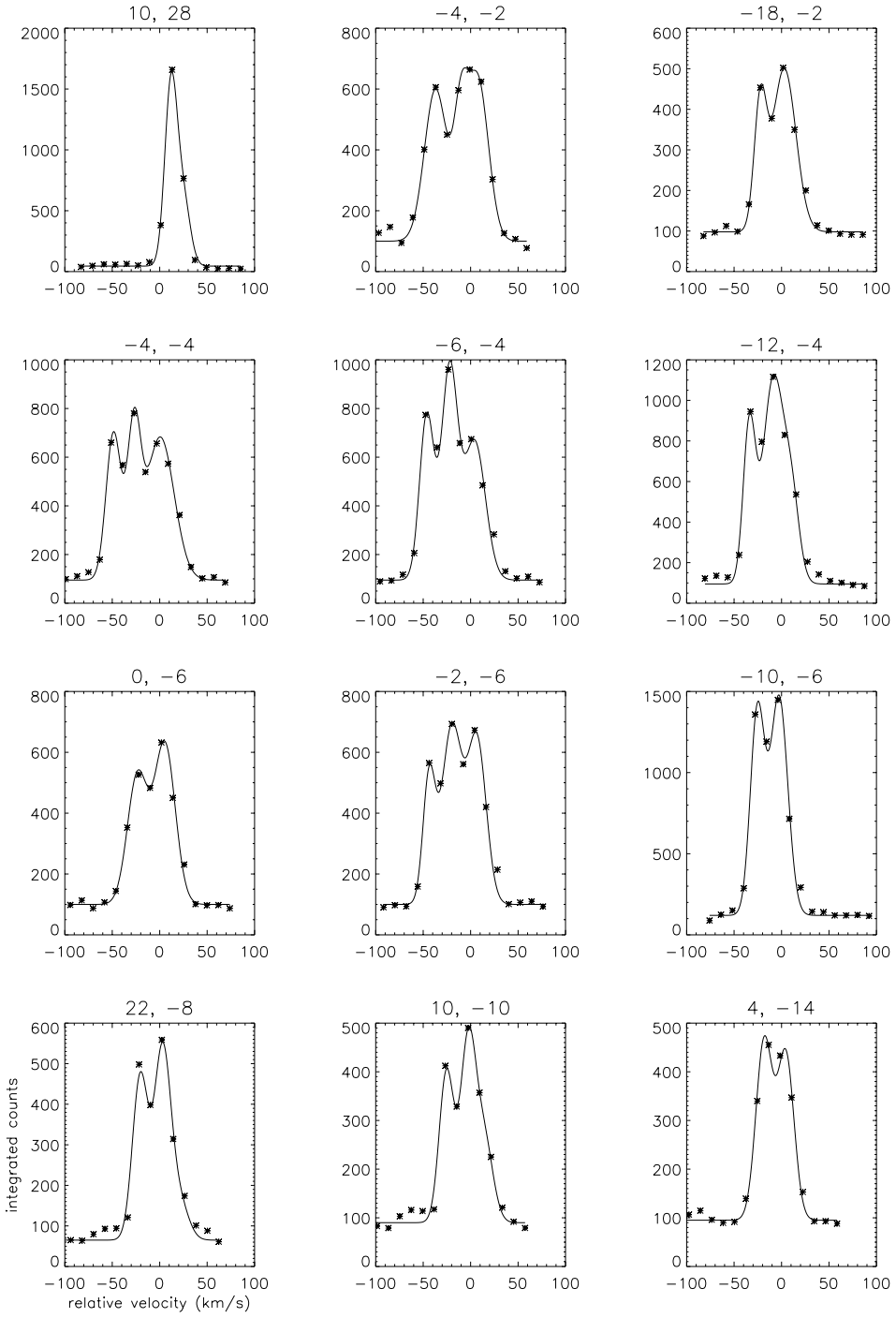

Fig. 2. A sample of the [OIII]5007Å profiles at various spatial positions (given on top of each profile in arcsecs with reference to the star Her 36; positive is West in RA and South in Dec).

3.1. Expansion of the HII region in [OIII]

Expansion is an important phase in the evolution of an HII region embedded in a giant molecular cloud, such as the HG. If found, it tells us that the ionization front is still destroying the surrounding molecular cloud and that the pressure equilibrium between the ionized and neutral media is not yet established. The observed kinematic differences between the NHG, the SHG and the region west of Her 36 seem to indicate considerable expansion in the HG region. As already mentioned, mass flows of positive velocities upto +15 km s^{-1} were observed towards the NHG, in contrast to those having negative velocities upto -35 km s^{-1} seen in a region south of Her 36. Further, split profiles with components separated by 20 to 30 km s^{-1} were found in the SHG. The split profiles (Fig. 2) observed towards the SHG and to the south of Her 36 could be due to two flows along the line of sight, having different Doppler velocity peaks. Earlier on, it was proposed by some authors (Dyson 1975; Dopita et al. 1974) that the split profiles are indicative of the presence of partially ionized globules (PIGs). However, splits of more than 20 km s^{-1} found here may need an alternative explanation.

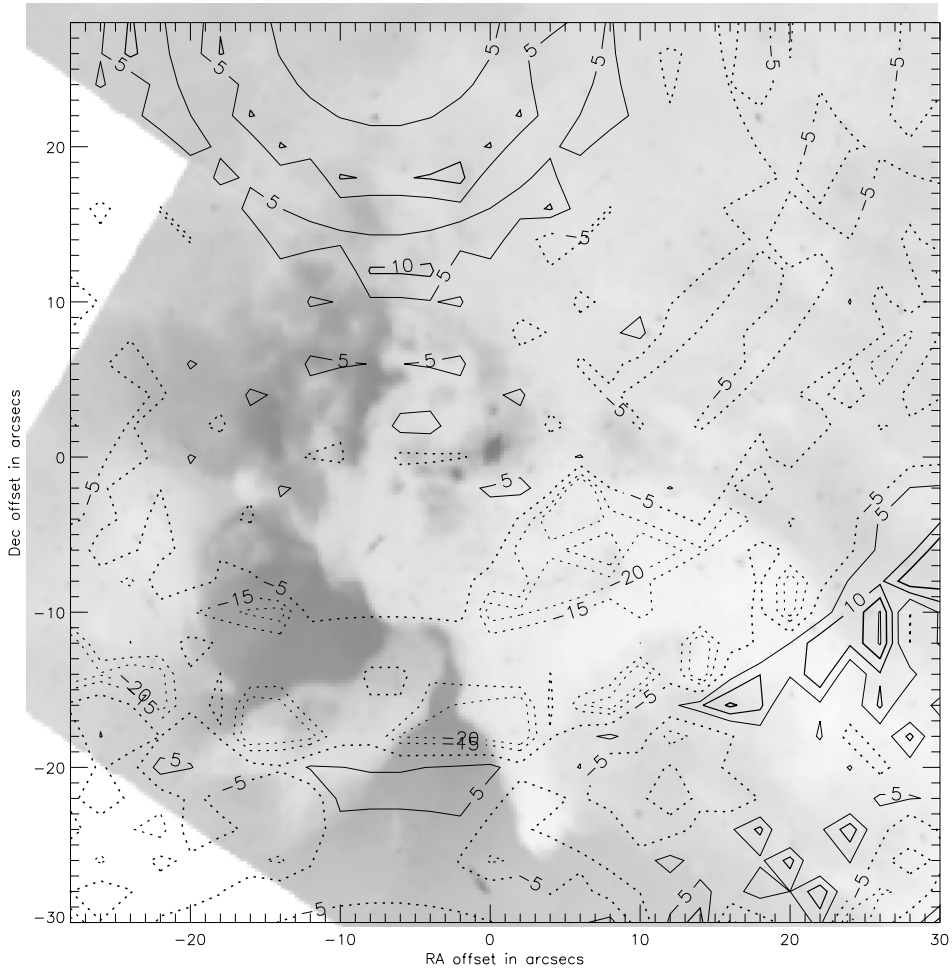

Fig. 3. [OIII]5007Å velocity field of the Hourglass region. The values show heliocentric velocities. The [OIII] image taken from HST archive is also shown (in negative) superposed on the velocity map. The diffuse dark spot at (0,0) is Her 36. North is up and East is to the left.

Yorke et al. (1984) showed in their model computations that the line splits are "not always indicative of blobs or filaments". These authors suggested that the splits could be "a result of a point of inflection in the projected line of sight velocity", leading to longer integration paths at a particular Doppler-shifted velocity. At some positions, especially towards the south-east of Her 36, more complex, three-component line profiles were observed, indicating the presence of multiple flows overlapping along the line of sight. The HST [OIII] overlap shows clumps of emitting matter occurring at about the same position as the multiple profiles. Such a complex structure was also found in CO emission lines (White et al. 1997). It should be pointed out that one of the components in the double-peaked line profiles is red-shifted while the other is blue-shifted with respect to Her 36. The positive component of the split line profiles could be due to the receding flow going into the cavity of SHG. Thus, the split profiles observed towards SHG and the south of Her 36 show an evidence of rapid expansion of the Her 36 bubble.

A moderate velocity of $-17\,\mathrm{km\,s^{-1}}$ was detected towards the west of Her 36. However, we do not find split profiles in this region. This could be due either to the absence of one of the flows or to the fact that the projected velocity separations of the components could be much less than twice the sampling stepsize of $12\,\mathrm{km\,s^{-1}}$. A similar situation prevails in the region of NHG except that in there, the line of sight velocities are positive. We find velocities of 10 to $15\,\mathrm{km\,s^{-1}}$ towards the northern edge of the HG. The gradual change of velocities from $-5\,\mathrm{km\,s^{-1}}$ in the central HG to $15\,\mathrm{km\,s^{-1}}$ in the NHG could be due to the orientation of cavities. If the opening of the cavity covering the portions of the central HG and NHG is perpendicular, then the projected velocity of the flow entering the cavity should be small. Our observations further suggest the presence of a cavity towards the northern edge of HG into which the matter is flowing with velocities of 10 to $15\,\mathrm{km\,s^{-1}}$.

It may be appropriate to compare the results on the [NII] velocity field obtained by CA with the [OIII] results presented here, with some caution due to the fact that the former has a lower spatial sampling but higher spectral resolution than the latter. We find that there is a general agreement between the two results, although the [NII] field shows higher velocities w.r.t the star Her 36. This can be attributed to the velocity stratification found also in several other HII regions like the Orion nebula(Dopita et al. 1974; O'Dell 1994). Such a stratification can be demonstrated by computing the regions of maximum emission for dominant ions. Using the photoionization code CLOUDY (version 90.4), we have computed the radial distribution of the volume emissivities of the Hα, [OIII], [NII], and [SII] lines. A filling factor of unity was assumed in a spherically symmetric nebula with

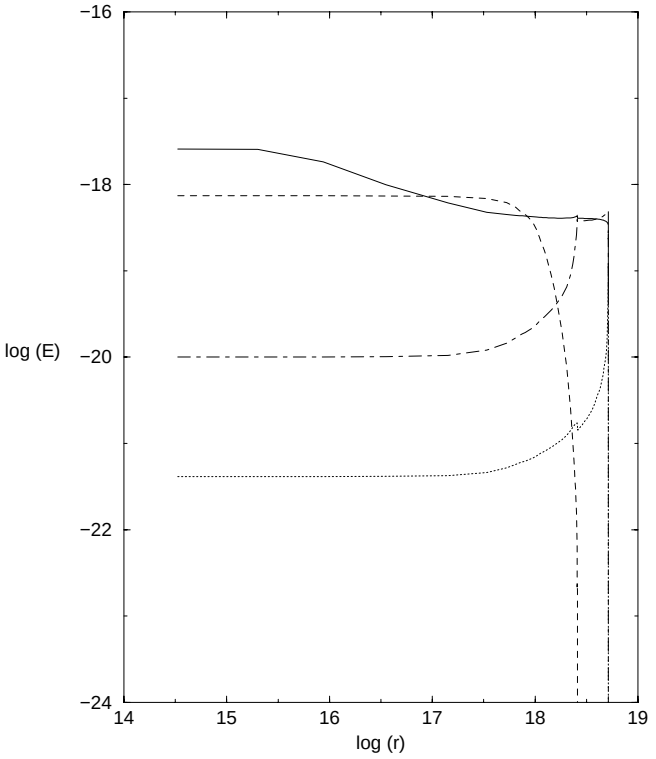

Fig. 4. Volume emissivity E (in ergs/cm^3/sec) as a function of radial distance (in cm) for Hα(solid curve), [OIII](dashed), [NII](dash-dotted), and [SII](dotted) lines.

the same elemental abundances as those in the Orion nebula and a particle number density of $1000\,\mathrm{cm}^{-3}$ centered around Her 36. Although the spherical symmetry is an over-simplified assumption, it represents reasonably well the expanding front of the region (i.e., the Champagne flow). Fig. 4 shows a plot of the volume emissivity distribution for various ions. We find that the [NII] emission is most prominent in a rather spatially thin region within which the [OIII] emission strength falls very steeply. In spite of this spatial stratification, one common feature in the velocity fields of the two ions (CA and the present work) is the expansion of gas around Her 36.

The heliocentric velocity of the neutral component was given by Goudis & Meaburn (1976) as $-1\,\mathrm{km\,s}^{-1}$. This is in good agreement with the value for the CO lines that can be deduced from the results of White et al. (1997), assuming that their value represents lsr value (Elliot et al. (1984) give $v_{lsr} = v_{hel} + 11.7\,\mathrm{km\,s}^{-1}$). In comparison, our value for the [OIII] is $-5\,\mathrm{km\,s}^{-1}$ in the Her 36 region. It appears, therefore, that there is no substantial relative velocity between the neutrals and ions. However, the internal motions are quite significant relative to the star Her 36 for both the species which can be interpreted, in both cases, as expansion of the nebula. White et al. (1997) chose to interpret the extended wings of molecular CO line profiles as indicative of expansion rather than outflows of shock origin (note the absence of molecular hydrogen emission). Hence, these results (ours and those of White et al.'s) broadly agree with the 3-D model due to Woodward et al. (1986).

3.2. High velocity regions and champagne flow

The present observations of [OIII] reveal some high velocity flows at certain places manifested as the primary components in the line profiles. As mentioned earlier, we find high velocity flows, upto $-30\,\mathrm{km\,s}^{-1}$ w.r.t. Her 36, towards the south of Her 36 near the southern lobe of the HG. Dyson (1975) showed that the flows from partially ionized globules could not possibly account for velocities larger than the local sound speed($\sim 10\,\mathrm{km\,s}^{-1}$). Alternatively, the high velocities may be attributed to the interaction of the expanding ionization front with the low density regions. Franco et al. (1990) showed that an expanding HII region can give rise to velocities up to $50\,\mathrm{km\,s}^{-1}$ while encountering a cloud edge, depending upon the steepness of the negative density gradient. Such a flow is termed as *Champagne* flow (Tenorio-Tagle 1979; Yorke et al. 1984; Yorke 1986). Thus, the high velocities particularly observed south of Her 36 (Fig. 3) indicate the presence of Champagne flow in the HG region. More recently, stellar winds from OB stars are shown to play a significant role in shaping the HII regions (Garcia-Segura & Franco 1996; Comeron 1997), especially in producing much higher velocities and greater blow-up sizes than the models which consider the Champagne flow only. However, the projected velocities observed by us are within the limits of the maximum velocities expected from the Champagne flow models. Therefore, while it is certainly possible that the stellar winds might have contributed to the shaping of the HII region, it may be unlikely that the observed high velocity flows are due to the winds.

It may be noted here that the high velocity flows reported by CA in the [NII] line observations were seen in the secondary components, in contrast with the [OIII] results. This can possibly be attributed to the fact that the two lines arise in two different regions having different physical conditions in the two emitting volumes (Yorke et al. 1984).

From the work of Woodward et al. (1986), it is evident that the HG region suffers spatially varying extinction which leads to the appearance of the HII region differently in different emission lines. These authors point out further that the [OIII] line suffers 2.7 times more attenuation in the NHG region than in the SHG region. It is therefore quite possible that the differential extinction could play a significant role in shaping the line profiles. Unless the extinction measurements are also available at high spatial resolution, modelling of the line profiles becomes considerably inaccurate.

3.3. Turbulence

Turbulence in interstellar matter was inferred when random spatial variations in radial velocity were detected (Münch 1958). Further, the width *W* of emission lines is usually much larger than the thermal component and the contribution due to expansion, if present. If the mass flow gradients and expansion are removed, then the line width can be decomposed as (Münch 1958):

$$W^2 = W^2_{thermal} + W^2_{turbulence} \quad (1)$$

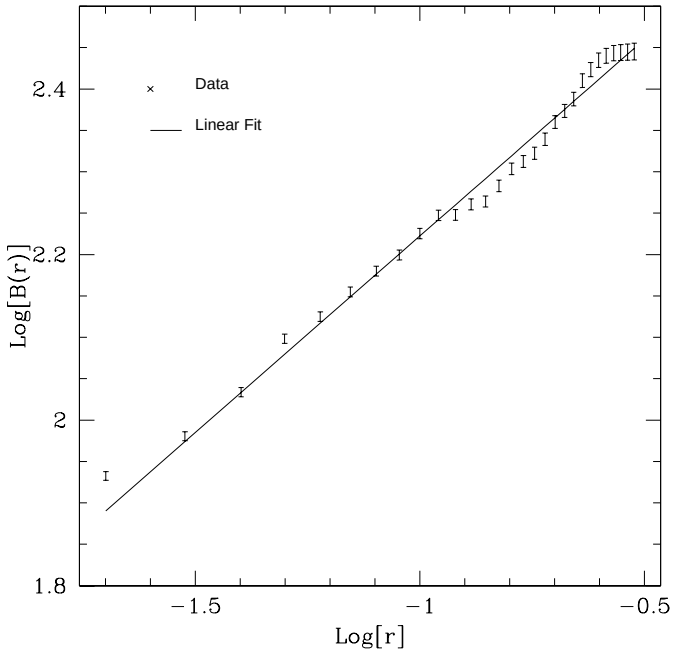

Fig. 5. The structure function $B(r)$ is shown as function of linear separation of the velocities observed towards the HG region. The velocities correspond to the peak positions (of the primary components) of the observed [OIII]5007Å line profiles.

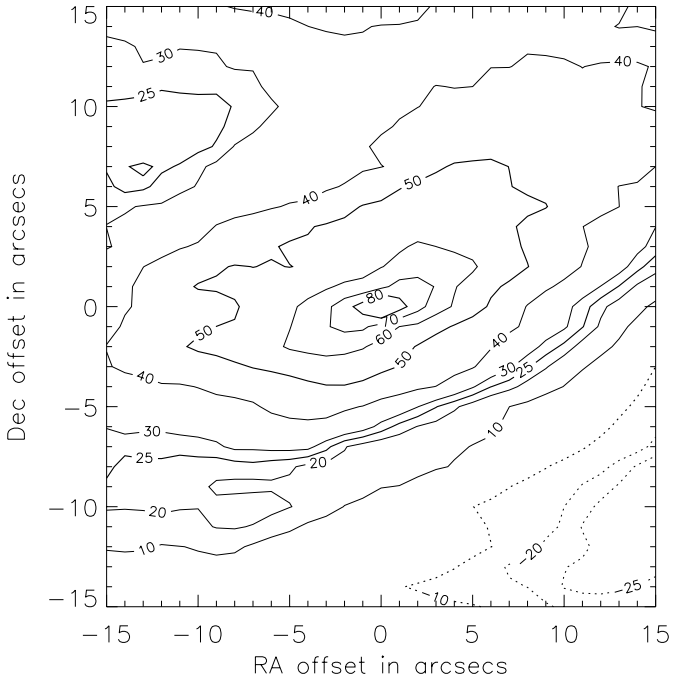

Fig. 6. The 2-dimensional autocorrelation function (ACF) around Her 36. The $X-$axis and $Y-$axis are the lags in arcsecs in RA (positive West) and Dec (positive North) respectively. The values on the contours should be divided by 100. The correlations are w.r.t. the central star. The full curves are positive correlations and the dotted curves at the bottom right corner are negative correlations.

The works of Roy & Joncas (1984, 1985), O'Dell (1986) and Castaneda (1988) showed quantitative evidence for the presence of turbulence in HII regions. A second order structure function $B(r)$ can be defined as follows (assuming it to be independent of position and direction in space, Kaplan & Kahn 1966):

$$B(r) = \overline{[v(r') - v(r'')]}^2 \quad (2)$$

The structure function $B(r)$ is a good measure of fine scale motions across the nebula. It involves differences of radial velocity at neighboring points separated by the scale size *r*=*r*′-*r*″ and thus the systematic flows are normalized to a greater extent. The correlation is based on the following assumptions: (a) that the turbulence is homogeneous and isotropic, (b) that the fluid is incompressible (constant density), and (c) that the sharp discontinuities in the gas motions like shock waves are neglected.

The correlation method was successfully applied to a number of HII regions like M42 (Münch 1958; Castaneda 1988), M 8 (O'Dell et al. 1987), and S142 and M17 (Roy & Joncas 1985; Joncas & Roy 1986). These authors pointed out that small scale velocity fluctuations and inadequate number of data points for the larger scale sizes can affect the accuracy of determination of the structure function and define its limit.

We determined the structure function in the HG region using 3721 velocity points (representing the primary components) derived from a grid of 61″×61″ of the [OIII] observations at a spatial resolution of 1″, for the sake of better statistical weightage. First we computed the function without removing systematic flows or velocity gradients from the data. Then we removed these components by systematically combing the data using a linear kernel of size varied from 2 to 4 arcsec in different combinations all over the velocity field and subtracting velocities in excess of half the instrumental width, namely 6 km s^{-1}. The resultant 'gradient-free' velocity map was then used to obtain the structure function. The difference between the two computations was found to be significant only at large scale sizes. Table 1 gives values of *B(r)* at different *r* along with number of points *N* considered. The largest scale size considered was 30″ with 900 possible combinations. Though the data points are at 1″ resolution, we took the smallest values for *r* to be 2″ due to the seeing limitations. Thus, *r* was varied from 2″ (0.02 pc) to 30″ (0.30 pc). Scale sizes larger than 30″ were not considered because of the smaller number of data points. A plot of $log(r)$ versus $log(B(r))$ is shown in Fig. 4. The errors in the structure function are estimated by using the relation $\delta B(r) = B(r)/\sqrt{N}$. The uncertainty in velocity centroiding being approximately the same at all positions, the uncertainty in $B(r)$ is assumed to be solely decided by the number of samples considered for its computation.

We found the slope to be 0.46, in quite contrast with the theoretically expected value of 2/3 or 0.67 (Kaplan & Kahn 1966). The possible reasons for the discrepancy can be that the nebular gas may not satisfy the assumptions made for the determination of the structure function. Further, it can be noticed from the figure that there could be different gradients at different ranges of scale sizes. The slope seems to steepen after a particular value of $r \sim 0.12$ pc ($\sim$ 15 arcsec). Such a trend was also reported in the earlier studies on other HII regions, indicating that the

Table 1. The structure function for different values of *r*.

r(arcsecs)	*B(r)*(km^2 sec^{-2})	*N*(total points)	*r*(arcsecs)	*B(r)*(km^2 sec^{-2})	*N*(total points)
2	85	3364	16	201	1936
3	95	3249	17	205	1849
4	108	3136	18	210	1764
5	125	3025	19	218	1681
6	133	2916	20	229	1600
7	142	2809	21	236	1521
8	151	2704	22	244	1444
9	158	2601	23	257	1369
10	168	2500	24	265	1296
11	176	2401	25	272	1225
12	176	2304	26	275	1156
13	182	2209	27	277	1089
14	183	2116	28	277	1024
15	191	2025	29	278	961
			30	278	900

turbulent energy is input at more than one scale size. It is important to note here that O'Dell's (1986) study of turbulence showed that the slope varies from 0.18 to 0.45 for different HII regions, in sharp contrast to the theoretically expected value of 0.67. O'Dell et al. (1987) obtained a similar value for the region around 9 Sgr in M 8, like the one obtained by us for the HG region.

Alternatively, the change in the slope of $B(r)$ beyond 0.12 pc could be due to large scale velocity gradients which remained possibly as residuals inspite of our attempt to remove the gradients. It was suggested by Kleiner & Dickman (1985) that the 2-Dimensional (2-D) autocorrelation function (ACF) would be able to bring out well such residual gradients if present in the velocity fields. We have computed the ACF for our velocity field in the region of $30'' \times 30''$ around Her 36 using the methodology of Kleiner & Dickman (1985). Fig. 6 shows the 2-D ACF around Her 36. The $X-$axis and $Y-$axis are the lags (in arcsec) in the RA and Dec. Note the extent of significant values (1/e value = 0.36) of the ACF stretching upto about $30''$ in RA but limited to $10'' - 15''$ in Dec. The average 1/e value turns out to be $\sim$ 15 arcsec ($\sim$ 0.12 pc). Notice also the significant correlations at the outer regions in the north-east region and the anti-correlations in the south-west regions. The anti-correlation regions suggest the presence of residual large scale velocity gradients (cf. the large negative velocities in Fig. 3). We conclude from Figs. 5 and 6 that the turbulence characterization upto about 0.12 pc around Her 36 is well brought about by $B(r)$ but the change in the gradient beyond that value (Fig. 5) could be due to residual large scale velocity gradients.

The source of turbulence in HII regions is an open topic. It is clear that turbulence needs a constant supply of energy to survive. Such energies usually come from velocity fluctuations causing shear in the mean flow (Tennekes & Lumley 1972). Density fluctuations within the medium can also cause velocity fluctuations. A clumpy medium can thus be a source of turbulence. Based upon the work of Scalo (1984), Roy & Joncas (1985) argued that the Kelvin-Helmholtz instability can be a cause of turbulence in HII regions with evolved Champagne flow (like in S142). However, they have shown that such a process needs $\leq 10^6$ years to grow. Since the age of HG region is estimated to be a few times 10^4 yr (Woolf 1961; CA), it is unlikely that such a process is the principal cause for the generation of turbulence in the HII region of Her 36. The other possible cause for the generation of turbulence could be the clumpiness of the HII region of Her 36. The shear between the flows of ionized matter from dense clumps (or partially ionized globules) can give rise to a turbulent medium (Roy & Joncas 1985).

4. Conclusions

The important conclusions of the paper are as follows:

1. New, seeing-limited [OIII] velocity field observations on the Hourglass region of M 8 were made using an Imaging Fabry-Perot Spectrometer.
2. The observations showed expansion of the HII region and high velocities up to $-35\,\mathrm{km\,s^{-1}}$ indicating Champagne flows. These results are in general agreement with our earlier observations on [NII] velocity field.
3. Our results showed three kinematically distinct regions in and around the HG.
4. The structure function characterizing the turbulence in the HG region showed a power index of 0.46. We find a distinct indication that the index steepens beyond the scale size of about 0.12 pc. However, the steepening could as well be due to residual velocity gradients as indicated in our 2-D ACF map.

Acknowledgements. We thank R.T. Patel and C. Muthu for their help during observations. This work is supported by the Department of Space, Govt. of India. We thank Prof. Gary Ferland for providing the CLOUDY code to the community at large. We thank the anonymous referee for having brought our attention to the 2-D ACF and for many other constructive comments on an earlier version.

References

Anandarao B.G., Rao S.R., 1985, BASI 14, 34
Atherton P.D., Taylor K., Pike C., et al., 1982, MNRAS 201, 661
Bohuski T.J., 1973, ApJ 183, 851
Castaneda H.O., 1988, ApJS 67, 93
Chakraborty A., 1997, Ph.D Thesis, Gujarat University, Ahmedabad (unpublished)
Chakraborty A., Anandarao B.G. 1997, AJ 114, 1576 (CA)
Comeron F., 1997, A&A 326, 1195
Dopita M.A., Dyson J.E., Meaburn J., 1974, Ap&SS 28, 61
Dyson J.E., 1975, Ap&SS 35, 299
Elliot K.H., Goudis C., Hippelein H., et al., 1984, A&A 138, 451
Franco J., Tenorio-Tagle G., Bodenheimer P., 1990, ApJ 349, 126
Garcia-Segura G., Franco J., 1996, ApJ 469, 171
Georgelin Y.M., Georgelin Y.P., 1976, A&A 49, 57
Goudis C., Meaburn J., 1976, A&A 51, 401
Hanel A., 1987, A&A 176, 338
Joncas G., Roy J.R., 1986, ApJ 307, 649
Kaplan S.A., Kahn F.D., 1966, Interstellar Gas Dynamics. Pergamon Press
Kleiner S.C., Dickman R.L., 1985, 295, 466
Lada C.J., Gottlieb C.A., Gottlieb E.W., et al., 1976, ApJ 203, 159
Lang K.R., 1991, Astrophysical Data. Springer-Verlag
Münch G., 1958, Rev.Mod.Phys. 30, 1035
O'Dell C.R., 1986, ApJ 304, 767
O'Dell C.R., 1994, ApSS 216, 267
O'Dell C.R., Townsley L.K., Castaneda H.O., 1987, ApJ 317, 676
Roy J.R., Joncas G., 1984, ApJ 283, 640
Roy J.R., Joncas G., 1985, ApJ 288, 142
Scalo J.M., 1984, ApJ 277, 556
Seema P., Anandarao B.G., Banerjee D.P.K., et al., 1992, PASP 104, 1091
Tenorio-Tagle G., 1979, A&A 71, 59
Tennekes H., Lumley J.L., 1972, A First Course in Turbulence, Cambridge
van Altena W.F., Jones B.F., 1972, A&A 20, 425
White G.J., Tothil N.F.H., Matthews H.E., et al., 1997, A&A 1997, 323, 529
Woolf N.J., 1961, PASP 73, 206
Woodward C.E., Pipher J.L., Helfer H.L., et al., 1986, AJ 91, 870
Woodward C.E., Pipher J.L., Helfer H.L., et al., 1990, ApJ 365, 252
Yorke H.W., Tenorio-Tagle G., Bodenheimer P., 1984, A&A 138, 325
Yorke H.W., 1986, ARA&A 24, 49